Synthesis and Characterization of Bis(2,2′-bipyridyl)platinum(I): A Novel Microtubular Linear-Chain Complex

ARTICLE *in* JOURNAL OF THE AMERICAN CHEMICAL SOCIETY · DECEMBER 1996

Impact Factor: 12.11 · DOI: 10.1021/ja962491m

4 AUTHORS, INCLUDING:

D. Brent Macqueen
SRI International
39 PUBLICATIONS **1,117** CITATIONS
SEE PROFILE

Cortlandt Pierpont
University of Colorado at Boulder
200 PUBLICATIONS **8,119** CITATIONS
SEE PROFILE

Synthesis and Characterization of Bis(2,2′-bipyridyl)platinum(I): A Novel Microtubular Linear-Chain Complex

Roger Palmans,[†,§] D. Brent MacQueen,[†] Cortlandt G. Pierpont,[‡] and Arthur J. Frank*[,†]

Contribution from the National Renewable Energy Laboratory, Golden, Colorado 80401, and Department of Chemistry and Biochemistry, University of Colorado, Boulder, Colorado 80303

Received July 18, 1996[⊗]

Abstract: One-electron reduction of $[Pt(bpy)_2]^{2+}$ (bpy = 2,2′-bipyridyl) in aqueous solution results in the formation of black-green lustrous needles on solid electrodes. The crystalline needles grow perpendicularly from the substrate surface and reach lengths of 1−2 cm. Elemental analysis, X-ray photoelectron spectroscopy, and electrochemical measurements indicate that the new compound is a genuine Pt^{I} complex with a d^9 electronic configuration and with the composition $[Pt(bpy)_2]NO_3 \cdot 2H_2O$. X-ray crystallographic analysis shows that the crystalline needles consist of linear chains of discrete $[Pt^{I}(bpy)_2]$ units with a Pt−Pt distance of 3.563(1) Å and with each bipyridyl ligand overlapping face-to-face (eclipsed) with its nearest neighbor. At the monomeric level, the structure of $[Pt^{I}(bpy)_2]$ units exhibits a distorted square-planar configuration with structural parameters very similar to those of the parent Pt^{II} complex, $[Pt(bpy)_2](NO_3)_2 \cdot H_2O$. The new linear-chain compound was prepared by chemical and electrochemical methods. The resulting crystals are relatively stable in air but oxidize slowly over a period of weeks. Scanning electron microscopy reveals that the crystals are tubular with a hollow near-hexagonal morphology. Cooperative effects influence the optical and electrical properties of the crystals. Because of extensive solid-state interactions between stacked monomeric $[Pt^{I}(bpy)_2]$ units, the crystals absorb strongly over the whole visible region and far into the near infrared. Their room temperature electrical conductivity is relatively high, 10 Ω^{-1} cm^{-1}.

Introduction

For several decades there has been considerable interest in linear-chain transition-metal complexes because of their unusual and highly anisotropic optical, electrical, and magnetic properties.[1−5] Their unusual properties arise, in part, from their unique lattice structure and cooperative interactions of monomeric units along the linear chain. Predominant among linear-chain materials are square-planar d^8 platinum complexes.[1,3,6−11] Because of their square-planar geometry, these materials can stack in one dimension. Linear-chain Pt compounds and Pt complexes have been of interest to us for some years because of their structure−property relationships and as photosensitizers and photocatalysts for solar photochemical energy conversion.[12−14] Interactions between Pt^{II} centers take place through orbitals of the metal, oriented along the *z* axis (d_{z^2} or p_z),[15] although ligand−ligand interaction between monomeric units can also occur.[16] Because of cooperative effects, spectral properties of linear-chain complexes in the solid state can be quite distinct from those of their individual monomeric constituents in solution. Many solid Pt^{II} complexes, such as Magnus' green salt $[Pt(NH_3)_4][PtCl_4]$, have intense electronic transitions in the visible spectrum that are not observed in the isolated monomeric complexes.[17] Interaction among adjacent monomeric units in the solid-state lattice of linear-chain complexes can result in substantial electron delocalization, producing richly colored materials. In linear-chain Pt^{II} systems, where direct Pt−Pt interactions occur, the intensity and wavelength maxima of the electronic spectrum depend linearly on the Pt−Pt distance.[3,18] Above a Pt−Pt spacing of about 3.6 Å, only the color of individual monomeric units is observable. With decreasing Pt−Pt distances, a broad, intense long-wavelength absorption appears, resulting in the characteristic color of the solid material. Cooperative effects also influence the electrical conductivity, which spans a wide range of values, from 10^3 to 10^{-12} Ω^{-1}

[†] National Renewable Energy Laboratory.
[§] Present address: IMEC, Kapeldreef 75, B-3001 Leuven, Belgium.
[‡] University of Colorado.
[⊗] Abstract published in *Advance ACS Abstracts,* December 1, 1996.

(1) *Extended Linear Chain Compounds*; Miller, J. S., Ed.; Plenum Press: New York, 1983; Vol. 1−3.
(2) Ward, M. D. In *Electroanalytical Chemistry*, Bard, A. J., Ed.; Marcel Dekker: New York, 1989; Vol. 16, p 181.
(3) Thomas, T. W.; Underhill, A. E. *Chem. Soc. Rev.* **1972**, *1*, 99.
(4) *Electronic Properties of Quasi-One Dimensional Compounds, Part I: Theoretical*; Monceau, P., Ed.; D. Reidel Publishing Co.: Dordrecht, 1985.
(5) *Lower-Dimensional Systems and Molecular Electronics*; Metzger, M. R., Day, P., Papavassiliou, G. C., Eds.; Plenum Press: New York, 1990.
(6) Miller, J. S.; Epstein, A. J. *Prog. Inorg. Chem.* **1976**, *20*, 1.
(7) *Chemistry and Physics of One-Dimensional Metals*; Keller, H. J., Ed.; Plenum Press: New York, 1977.
(8) *Extended Interactions between Metal Atoms*; Interrante, L., Ed.; American Chemical Society: Washington, DC, 1974.
(9) *Low Dimensional Cooperative Phenomena*; Keller, H. J., Ed.; Plenum Press: New York, 1975.
(10) Hone, D. W.; Richards, P. M. *Annu. Rev. Mater. Sci.* **1974**, *4*, 337.
(11) Krogman, K. *Angew. Chem., Int. Ed. Engl.* **1969**, *8*, 35.
(12) (a) Houlding, V. H.; Frank, A. J. *Inorg. Chem.* **1985**, *24*, 3664. (b) Houlding, V. H.; Frank, A. J. In *Homogeneous and Heterogeneous Photocatalysis*; Pelizetti E., Serpone, N., Eds.; NATO ASI Ser., Ser. C, 1986; Vol. 174, pp 199−211. (c) Honda, K.; Chiba, K.; Tsuchida, E.; Frank, A. J. *J. Mater. Sci. Lett.* **1989**, *24*, 4004.
(13) Palmans, R.; Frank, A. J.; Houlding, V. H.; Miskowski, V. M. *J. Mol. Catal.* **1993**, *80*, 327.
(14) (a) Palmans, R.; Frank, A. J. *J. Phys. Chem.* **1991**, *95*, 9438. (b) Craig, C. A.; Garces, F. O.; Watts, R. J.; Palmans, R.; Frank, A. J. *Coord. Chem. Rev.* **1990**, *97*, 193.
(15) Reference 8, Chapters 18 and 19.
(16) Schneider, O.; Metz, J.; Hanack, M. *Mol. Cryst. Liq. Cryst.* **1982**, *81*, 273.
(17) Fleischauer, P. D. In *Concepts of Inorganic Photochemistry*; Adamson, A. W., Fleischauer, P. D., Eds.; John Wiley: New York, 1975; p 398.
(18) Keller, H. J. In ref 1, Vol. 1, p 401.

S0002-7863(96)02491-2 CCC: $12.00

cm^{-1}.[19] Most linear-chain materials are rather poor conductors, reminiscent of semiconductors or insulators. In the case of one-dimensional conductors, charge transport occurs predominantly along the molecular chain and can involve electron delocalization through metal−metal or ligand−ligand overlap. A number of linear-chain compounds can be synthesized electrochemically, resulting in the production of thin needle-like crystals, such as $K_{1.75}Pt(CN)_4 \cdot 1.5\ H_2O$, with conductivity highest in the direction of growth.[20] Cooperative magnetic effects have also been observed. They result from spin interactions between monomeric units and can give rise to either ferromagnetic or antiferromagnetic behavior.[21]

Combining the anisotropic properties of linear-chain transition-metal complexes with a tubular morphology could lead to the design of molecular based electronic or photonic devices and novel catalytic materials. The possibility of forming such structures from linear-chain transition-metal complexes has not been reported. Formation of tubular structures has been demonstrated for carbon based fullerenes,[22,23] binary and ternary main group metals (e.g., In_2Te_3,[24] SbSeBr,[25] and SbSI[26]), and in the mineralization of self-assembling lipid tubules.[27] The fullerene and main group tubular materials have been grown from the vapor phase. Tubular materials (e.g., CdSe) have also been fabricated from molten salts.[28] The fabrication of tubular materials from discrete molecular species, such as transition-metal complexes, is anticipated to facilitate the tailoring of their physical and electronic properties through conventional synthetic chemistry.

In this article, we report on the synthesis and characterization of the first example of a linear-chain d^9 Pt^I complex that adopts a tubular macroscopic structure. Up until now, only linear-chain Pt complexes with a d^8 electronic configuration have been reported.[6] Moreover, platinum complexes with a d^9 electronic configuration have been shown[29−33] to form only dinuclear complexes with short Pt−Pt σ bonds. The linear-chain Pt^I complex of the present study was formed by the one-electron reduction of $[Pt^{II}(bpy)_2]^{2+}$ (bpy = 2,2′-bipyridyl) in aqueous solution and consists of discrete $[Pt^I(bpy)_2]$ units as shown by its crystal structure. We have characterized and investigated this material by UV−visible and near-infrared (IR) spectrophotometry, X-ray photoelectron spectroscopy (XPS), dc conductivity, and scanning electron microscopy (SEM).

Experimental Section

Materials. $[Pt^{II}(bpy)_2](NO_3)_2 \cdot H_2O$ was synthesized as reported elsewhere.[34,35] $[Pt^I(bpy)_2](NO_3) \cdot 2H_2O$ was prepared by both chemical and electrochemical methods. In the chemical procedure, 0.12 g (0.18 mmol) of $[Pt^{II}(bpy)_2](NO_3)_2 \cdot H_2O$ was dissolved in 5 mL of distilled H_2O containing 0.2 mL of 0.1 M HCl. The solution was sealed in a 10-mL Wheaton serum vial and deaerated by Ar bubbling for 15−20 min. An iron wire (5 cm × 0.25 mm, 99.998%, Aldrich) was then inserted through the septum, and the vial was sealed with hot wax and then placed in the dark. Over a period of 36 h, black-green shiny crystals of the Pt^I complex grew radially from the surface of the iron wire. The crystals were washed with deoxygenated H_2O and dried in a continuous stream of argon. Yields were typically greater than 95%. Elemental analysis gave good agreement with the expected values (mass percentages calculated for $[Pt^I(bpy)_2](NO_3) \cdot 2H_2O$ are quoted in parentheses): Pt, 31.60 (32.22); C, 39.30 (39.67); H, 3.14 (3.33); N, 11.50 (11.57); O, 13.49 (13.21); NO_3^-, 9.90 (10.24). Karl Fisher water analysis (Galbraith Laboratory) of the $[Pt^I(bpy)]$ complex gave a value of 5.65% (w/w), corresponding to 2 waters of hydration per mononuclear complex.

In the electrochemical method, $[Pt^I(bpy)_2](NO_3) \cdot 2H_2O$ needles were grown on transparent indium tin oxide conducting glass (ITO, 30−40 Ω/sq) or Pt wire (5 cm × 0.25 mm, 99.99%, Aldrich) electrodes by electrochemical reduction of $[Pt^{II}(bpy)_2](NO_3)_2 \cdot H_2O$ in a three-electrode, three-compartment cell consisting of a Pt-mesh counter electrode and a saturated calomel reference electrode (SCE); each compartment was separated by a medium porosity glass frit. Immediately before use, ITO electrodes were cleaned by immersing or rinsing them sequentially in aqueous 2% MICRO® detergent solution (10 s), distilled water, aqueous 2% HCl (20 s), distilled water, methanol (10 s), and distilled water. Typically, 0.35 g (0.58 mmol) of $[Pt^{II}(bpy)_2](NO_3)_2 \cdot H_2O$ was dissolved in 25 mL of 0.1 M $NaNO_3$. The solution was bubbled with Ar prior to crystal preparation. During electrochemical synthesis of the needles, the potential was held at −0.7 V, and a stream of Ar was maintained over the solution. The $[Pt^I(bpy)_2]$ needles grew perpendicularly to the electrode surface. The reaction was allowed to continue for 4−5 h. The black-green crystalline needles were collected on a medium porosity glass frit, washed with cold deoxygenated water, dried in a stream of Ar, and then stored in a Wheaton vial that was purged with Ar and kept in the dark. Yields were typically in the range of 70−80%. The density of crystals was evaluated by the flotation method to be 2.030 g/cm^3.

The resistivity of $[Pt(bpy)_2]$ crystals was measured by both four-point probe direct-current Van der Pauw and two-point probe methods. Electrical contacts were made with a GaIn eutectic. The concentration of free 2,2′-bipyridine (or Fe^{2+}) in solution was assessed spectrophotometrically by evaluating the quantity of $[Fe(bpy)_3]^{2+}$ formed from the reaction of bipyridine with Fe^{2+}.

Apparatus. Diffuse-reflectance spectra of the $[Pt(bpy)_2]$ complexes were measured with a Perkin-Elmer Lambda 9 UV−visible near-IR spectrophotometer with a MgO integrating sphere. Absorbance measurements of solutions were obtained with a HP 8450A diode-array spectrophotometer. Current−voltage measurements utilized a Princeton Applied Research (PAR) Model 173 potentiostat, PAR Model 175 universal programmer, and PAR Model 179 digital coulometer system. Hydrogen was measured on a Gow Mac 550P gas chromatograph (GC) equipped with a thermal conductivity detector, a 5-Å molecular sieve column, and argon carrier gas. XPS was conducted with a Surface Science Model SSX-100 ESCA system, having a base pressure of 6.7×10^{-7} Pa (5×10^{-9} Torr). XPS data were obtained with Al Kα radiation and a 100-eV pass energy setting, corresponding to a curve-fitted energy resolution of 0.16 eV/channel.

X-ray crystallographic measurements of $[Pt(bpy)_2](NO_3) \cdot 2H_2O$ were carried out on a Siemens P3/F automated diffractometer. Mo Kα radiation (monochromatized by diffraction off a highly oriented graphite crystal) was used in this study. A crystal was mounted with epoxy on a glass fiber. Omega scans and axial photographs were used to verify that the crystal was not twinned. Photographs indicated orthorhombic symmetry, and the centered settings of 25 reflections were used to refine

(19) Carneiro, K. In *Electronic Properties of Inorganic Quasi-One-Dimensional Materials*; Monceau, P., Ed.; D. Reidel Publishing Co.: Dordrecht, 1985; Vol. 2, pp 1−68.
(20) Gliemann, G.; Yersin, H. *Structure and Bonding*; Springer-Verlag: New York, 1985; Vol. 62, p 87.
(21) Miller, J. S.; Epstein, A. J.; Reiff, W. M. *Science* **1988**, *240*, 40, and references therein.
(22) Saito, R.; Fujita, M.; Dresselhaus, G.; Dresselhaus, M. S. *Mater. Sci. Eng. B* **1993**, *B19*, 185.
(23) Dresselhaus, M. S.; Dresselhaus, G.; Satio, R. *Solid State Commun.* **1992**, *84*, 201.
(24) Kunjomana, A. J.; Mathai, E. *Mater. Res. Bull.* **1991**, *26*, 1347.
(25) Arivuoli, D.; Gnanam, F. D.; Ramasamy, P. J. *Mater. Sci. Lett.* **1987**, *6*, 249.
(26) Arivuoli, D.; Gnanam, F. D.; Ramasamy, P. J. *Cryst. Growth* **1986**, *79*, Pt. 1, 432.
(27) Archibald, D. D.; Mann, S. *Nature (London)* **1993**, *364*, 430.
(28) Minoura, H.; Negoro, T.; Kitakata, M.; Veno, Y. *Solar Energy Materials* **1985**, *12*, 335.
(29) Neve, F.; Ghedini, M.; Tiripicchio, A.; Ugozzoli *Organometallics* **1992**, *11*, 795.
(30) Uson, R.; Fornies, J.; Espinet, P.; Fortuno, C.; Milagros, T.; Welch, A. J. *J. Chem. Soc., Dalton Trans.* **1989**, 1583.
(31) Betz, P.; Bino, A. *J. Am. Chem. Soc.* **1988**, *110*, 602.
(32) Blau, R. J.; Espenson, J. H.; Kim, S.; Jacobson, R. A. *Inorg. Chem.* **1986**, *25*, 757.
(33) Arnold, D. P.; Bennett, M. A.; Bilton, M. S.; Robertson, G. B. *J. Chem. Soc., Chem. Commun.* **1982**, 115.
(34) Morgan, G. T.; Burstall, F. H. *J. Chem. Soc.* **1934**, 965.
(35) Livingston, S. E.; Wheelahan, B. *Aust. J. Chem.* **1964**, *17*, 219.

Table 1. Crystal Data, Data Collection Conditions, and Solution and Refinement Details for $[Pt^{I}(bpy)_2](NO_3)\cdot 2H_2O$

empirical formula	$C_{20}H_{20}N_5O_5Pt$
formula weight	605.49 g/mol
color, habit	black-green needles
temperature	150(2) K
radiation	Mo Kα ($\lambda = 0.71073$ Å)
crystal system	orthorhombic
space group	I222
unit cell dimensions	
a	3.563(1) Å
b	14.371(3) Å
c	19.232(4) Å
volume	984.8(4) Å^3
formula units/cell	$Z = 2$
mass density (calculated)	1.921 g/cm^3
mass density (measured)	2.030 g/cm^3
absorption coefficient	7.228 nm^{-1}
F(000)	586
crystal size	0.62 × 0.08 × 0.06 nm
θ range for data collection	1.5 to 27.50°
index ranges	$-4 < h < 4$, $-18 < k < 18$, $-25 < l < 25$
reflections collected	4530
independent reflections	1151 [R(int) = 0.0402]
refinement method	full-matrix least-squares on F^2
data/parameters	18.2
goodness-of-fit on F^2	0.85
final R indices [$I > 2\sigma(I)$][a]	$R = 0.027$, $R_w = 0.032$
R indices (all data)[a]	$R = 0.034$, $R_w = 0.045$
largest diff. peak and hole	0.314 and −0.202 e/Å^{-3}
absorption correction	empirical (psi scans)
transmission coeff.	max = 0.935, min = 0.589

[a] $R = \sum||F_o| - |F_c||/\sum|F_o|$; $R_w = [\sum w(|F_o| - |F_c|)^2/\sum w|F_o|^2]^{1/2}$.

the cell constants given in Table 1. A full sphere of redundant data was collected at 150 K and averaged to give 1151 independent observed reflections. A sharpened Patterson map was used to determine the location of the Pt atom at a site of 222 symmetry. A difference Fourier map revealed the positions of the six independent bipyridine ring atoms. A residual peak at 0,0,0, which is also a site of 222 symmetry, was refined as the nitrogen of the nitrate anion. A peak within a reasonable N−O bond length located along a crystallographic 2-fold axis was refined as one disordered half-oxygen of the nitrate. A second peak located at a site of 2-fold symmetry and separated from the nitrate oxygen by a distance appropriate for a weak hydrogen-bonding interaction was refined as the oxygen of a water solvate molecule. The site symmetry of the nitrate anion and the water oxygen atom results in a stacked network of nitrate anions and hydrogen-bonded water molecules. Imposed 222 symmetry at the location of the nitrate nitrogen disorders the remaining nitrate oxygens. They are not fixed in place by hydrogen bonding and their locations were not apparent, even on the difference Fourier calculated at the conclusion of the refinement. Tables containing details of the solution and refinement of the structure, anisotropic displacement parameters, and hydrogen atom locations are available as Supporting Information.

Results and Discussion

Very little is known about the chemistry of reduced $[Pt(bpy)_2]^{2+}$, particularly in aqueous solution. In *N*,*N*-dimethylformamide (DMF), the first reduction wave of $[Pt^{II}(bpy)_2]^{2+}$ is irreversible (−0.97 V vs SCE) and is ascribed to the conversion of Pt^{II} to Pt^{I}.[36,37] At potentials more negative than the metal-centered reduction, two reversible one-electron waves are observed[36,37] and are attributed[37] to consecutive one-electron reductions of bipyridyl ligand. The metal-centered reduction of $Pt(bpy)_2^{2+}$ appears to contrast with the ligand-centered reduction of $Pt(bpy)L_n$ ($n = 1$, bidentate ligand (excluding 2,2′-bipyridine); $n = 2$, monodentate ligand) in DMF.[38] In aqueous solution, the reduction of an analogous complex, $[Pt^{II}(phen)_2]^{2+}$, is reported[39,40] to give rise to the formation of an olive-green filamentous material on the surface of a mercury electrode or an iron wire. Isolation and identification of the material were, however, not possible.

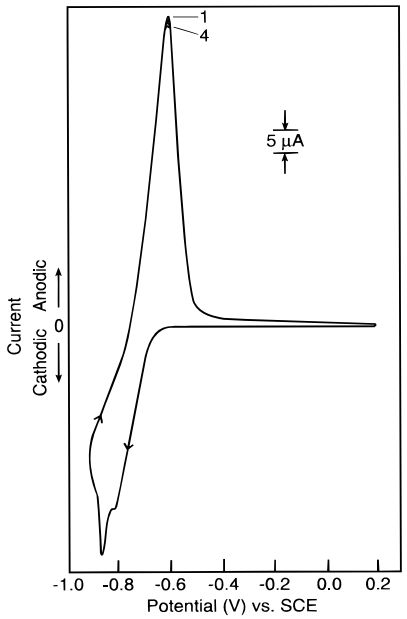

Figure 1. Cyclic voltammograms of 10^{-3} M $[Pt^{II}(bpy)_2]^{2+}$ in 0.1 M Na_2SO_4 with an ITO electrode; scan rate of 100 mV/s.

Figure 1 displays a cyclic voltammogram of 10^{-3} M $[Pt^{II}(bpy)_2](NO_3)_2\cdot H_2O$ in deaerated H_2O (pH 6)/0.1 M $NaSO_4$ with an ITO electrode in the potential range of 0.2 to −0.9 V. When the potential is scanned negatively from 0.2 V, a reduction peak at −0.84 V preceded by a shoulder at −0.80 V is seen. On reversal, an oxidation peak at −0.61 V is produced. The shapes and redox potentials of the waves displayed little change during cycling, although the magnitude of the peak currents showed a small progressive decrease. The cyclic voltammogram is not consistent with a simple reversible one-electron transfer. The nonunity value of the anodic-to-cathodic current ratio (1.1) and the large potential difference between peak currents (230 mV) indicate non-Nernstian behavior. The relatively positive potential at −0.84 V rules out one-electron reduction of the bipyridyl ligand. The reductive peak current varies linearly with the square root of the scan rate (5−200 mV/s), revealing that charge-transfer kinetics for reduction of $[Pt(bpy)_2]^{2+}$ are diffusion limited. In contrast, the oxidative peak current exhibits neither a square root nor a linear dependence on the scan rate, suggesting that the oxidation of reduced $[Pt(bpy)_2]^{2+}$ is limited by another process. This observation, along with the non-Nernstian behavior, is consistent with a surface-controlled process involving reduced $[Pt(bpy)_2]^{2+}$, as discussed below. When the ITO electrode is replaced by a Pt disk electrode, the cyclic voltammogram remains qualitatively the same; however, the respective reduction and oxidation waves occur at about −0.87 and −0.62 V.

To explore the adsorption phenomenon in more detail, we investigated the reduction process near the potential for the cathodic current maximum. Controlled potential electrolysis of 1.2×10^{-2} M $[Pt(bpy)_2]^{2+}$ in deaerated aqueous 0.5 M $NaNO_3$ solution resulted in the formation of black-green lustrous needles on the surface of a Pt wire electrode poised at −0.7 V.

(36) Chassot, L.; von Zelewsky, A. *Inorg. Chem.* **1987**, *26*, 2814.
(37) Braterman, P. S.; Song, J.-I.; Wimmer, F. M.; Wimmer, S. *Inorg. Chim. Acta* **1991**, *189*, 7.
(38) Braterman, P. S.; Song, J.-I.; Wimmer, F. M.; Wimmer, S.; Kaim, W.; Klein, A.; Peacock, R. D. *Inorg. Chem.* **1992**, *31*, 5084.
(39) Hall, J. R.; Plowman, R. A. *Austr. J. Chem.* **1956**, *9*, 143.
(40) Sundholm, G. *Suom. Kemistil.* (The Finnish Chemical Journal) **1969**, *10*, 401.

The crystalline needles grew radially from the electrode surface and reached lengths of 1−2 cm. The crystals can be isolated from the solution and appear stable in air for over a period of weeks. Eventually, exposure to air causes the crystals to turn from black-green to purplish-brown, implying that oxidation occurs. No change in color is noticed when the black-green crystals are stored in an argon or a nitrogen atmosphere. The formation of the crystals was independent of the electrolyte (Na_2SO_4, NaCl, or $NaNO_3$). Spectrophotometric analysis of the solution shows no evidence for the release of bipyridine during the growth of the crystals, indicating that the structure of the crystals contains the basic $[Pt(bpy)_2]$ moiety. At concentrations of $[Pt(bpy)_2]^{2+}$ of less than 10^{-3} M, crystals did not visibly form on the electrode surface, suggesting that their growth depends on the concentration of $[Pt(bpy)_2]^{2+}$ in solution. Similar crystal growth behavior occurs on ITO electrodes at a potential of −0.7 V.

When an ITO electrode is poised at potentials negative of about −0.8 V, the nature of the crystals growing from the electrode is altered. At potentials <-0.8 V, grayish-green hair-like needles grow perpendicularly from the electrode surface instead of the black-green ones observed at −0.7 V. Moreover, trapped gas, identified as H_2, forms within clusters of the needles at a potential of about 400 mV positive of the threshold potential for H_2 evolution at a bare ITO electrode, indicating that the crystals lower the overpotential for H_2 production. These crystals are quite sensitive to oxygen. When air is introduced into the electrochemical cell, they turn rapidly brown and solubilize in the solution. Moreover, minor vibrations of the electrochemical cell result in the detachment of the crystals from the electrode surface and their dissolution in either the presence or absence of oxygen. Spectrophotometric measurements of the resulting solutions showed a UV−visible spectrum characteristic of the original $[Pt(bpy)_2]^{2+}$ when O_2 is present. Because it was not feasible to isolate the crystals grown at potentials negative of −0.8 V, no further characterization of them was made.

To determine whether it was possible to grow the dark-green crystals on metals with an appropriate emf, we examined their growth behavior on iron. The emf value of Fe^{2+}/Fe is −0.68 V,[41] which is close to the condition for growing the crystalline needles on ITO or Pt wire electrodes. As expected, metallic iron, when exposed to $[Pt(bpy)_2]^{2+}$ in deoxygenated aqueous 3×10^{-4} M HCl solution, induces the formation of black-green shiny needles of the type grown electrochemically. When detached from the iron wire (or electrode), no further crystal growth occurs. This observation, along with their linear shape and perpendicular growth pattern, as in the case of electrochemically grown needles, indicates charge transport and reduction of $[Pt(bpy)_2]^{2+}$ occurs vectorially along the main axis of the crystals. The formation of crystals on the iron wire takes place only under acidic conditions. In neutral aqueous solutions, no crystal growth could be induced, even after several days. During the reaction in acidic solution, iron atoms at the surface of the wire are oxidized to Fe^{2+}, as confirmed by the appearance of the characteristic absorption spectrum of the $[Fe(bpy)_3]^{2+}$ complex when 2,2′-bipyridine was added to the supernatant after completion of the reaction. Elemental analysis (Experimental Section) showed that the crystals were composed of $[Pt(bpy)_2](NO_3)\cdot 2H_2O$.

Figure 2 shows scanning electron micrographs of crystalline needles of $[Pt^{I}(bpy)_2](NO_3)\cdot 2H_2O$ grown electrochemically. Analyses of several micrographs indicate that some of the crystals are hollow and others exhibit closed ends. The inner diameter of the hollow tubules typically varies from 10 to 40 μm with a wall thickness ranging from 2 to 8 μm. The same result was obtained for samples grown chemically on an iron wire. The vectorial growth pattern and high electrical conductivity (discussed below) of the crystals indicate that electron transfer to monomeric $[Pt(bpy)_2]^{2+}$ in solution occurs mainly at the leading edge of the tip of the crystals. Presumably, the presence of high energy surface features at nucleation (defect) sites on the substrate promotes selective adsorption of monomeric $[Pt(bpy)_2]^{2+}$ species and initiates localized crystal growth. The conditions for growing the crystals probably favor their hollow nature.[42] Specifically, the tubular morphology of the needles implies that the leading edge of the crystals grows at a faster rate than the central region, implying that the crystal edge is more reactive, which correlates with the edge of the tip having a smaller radius of curvature than that of the crystal wall. The faster growth at the edge also suggests a higher current density at the tip than along the wall of the crystal. This results in an extending-wall structure and a recessed central region of the crystal. Electron conduction through the needles of $[Pt^{I}(bpy)_2](NO_2)\cdot 2H_2O$ therefore occurs principally through the wall structure, perpendicularly to the substrate surface.

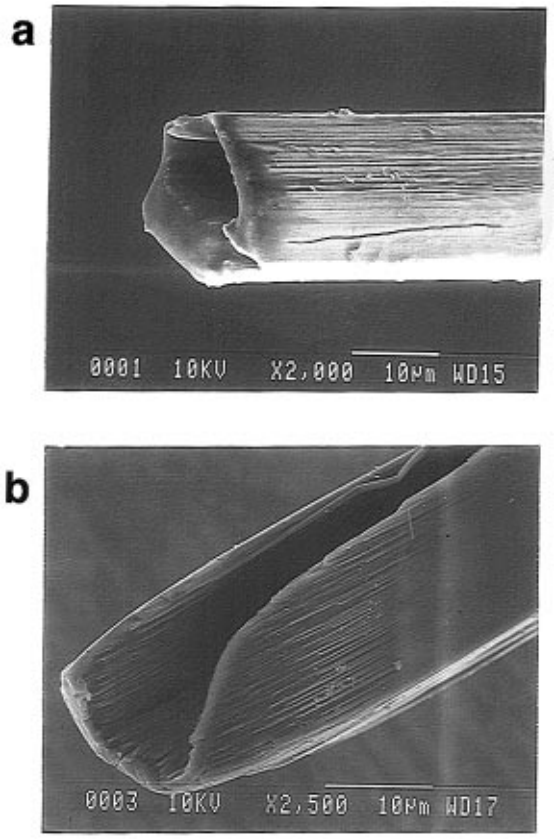

Figure 2. Scanning electron micrographs of $[Pt^{I}(bpy)_2](NO_3)\cdot 2H_2O$ showing (a) the near-hexagonal shape of a crystalline needle and (b) the hollow nature of a damaged needle.

Evidence for platinum being in the +1 oxidation state was obtained from high-resolution XPS of the black-green needles. Table 2 compares the binding energies of the Pt 4f core levels of the new Pt complex with those of the parent Pt^{II} complex and a Pt foil. The positions of the Pt 4f doublet of the crystals at 76.2 and 72.9 eV are 0.7 eV lower than that of $[Pt^{II}(bpy)_2](NO_3)_2\cdot H_2O$ at 76.9 and 73.6 eV, implying that the oxidation state of the Pt centers of the new complex is less than +2.

(41) Antelman, M. S. *The Encyclopedia of Electrochemical Electrode Potentials*; Plenum Press: New York, 1982.

(42) Ward, M. D., University of Minnesota. Personal communication.

Table 2. High-Resolution XPS Data: Binding Energies (eV) of Pt 4f Core Level of Pt Bipyridyl Complexes and Elemental Pt[a]

material	Pt $4f_{5/2}$	Pt $4f_{7/2}$
$[Pt^{II}(bpy)_2](NO_3)_2 \cdot H_2O$	76.9 (1.74)	73.6 (1.98)
$[Pt^{I}(bpy)_2](NO_3) \cdot 2H_2O$ (black-green needles)	76.2 (1.91)	72.9 (1.76)
Pt foil (ref 43)	74.5 (1.75)	71.2 (1.65)

[a] Full width at half-maximum values in parentheses.

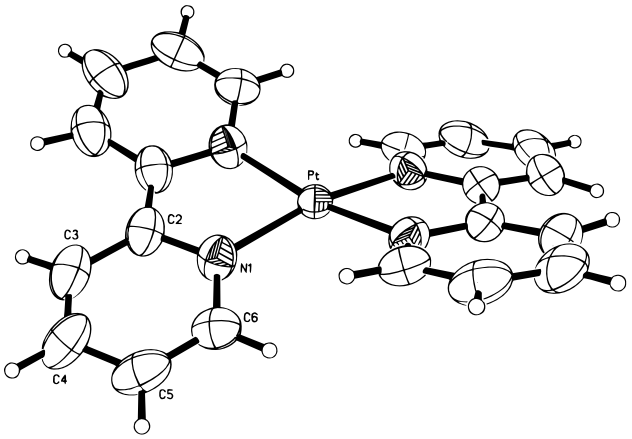

Figure 3. Thermal ellipsoid (50% probability) plot of the $[Pt^{I}(bpy)_2]$ monomeric unit in the linear-chain complex $[Pt^{I}(bpy)_2](NO_3) \cdot 2H_2O$ (with numbering scheme).

Similarly, the positions of the Pt core levels of the complex are 1.7 eV higher than that of Pt(0) at 74.5 and 71.2 eV,[43] indicating that the oxidation state of the Pt nucleus of the new complex is greater than 0. Furthermore, because only one Pt 4f doublet is observed in the XPS spectrum, a mixed-valence state structure can be ruled out. The full width at half-maximum (fwhm) values of the Pt 4f doublet concurs with these inferences. X-ray absorption near-edge spectroscopy (XANES) studies[44] of $[Pt(bpy)_2](NO_3)_2 \cdot H_2O$ and $[Pt(bpy)_2]NO_3 \cdot 2H_2O$ agree with the platinum of the latter complex being in the +1 oxidation state. The presence of only one NO_3^- counterion in the formula of the reduced complex (Experimental Section) is also consistent with a one-electron reduced metal center. Thus, XPS, XANES, and elemental analysis indicate that Pt centers of the black-green crystals are present predominantly in the +1 oxidation state and have a d^9 electronic configuration.

To obtain structural information, X-ray crystallographic measurements were made on $[Pt^{I}(bpy)_2](NO_3) \cdot 2H_2O$ crystals, grown on iron wires from $[Pt^{II}(bpy)_2](NO_3)_2 \cdot H_2O$ in deaerated aqueous 4×10^{-3} M HCl solution. Figures 3 and 4 show views of the $[Pt(bpy)_2]^+$ cation and the stacking interaction between cations in the crystal structure. Bond lengths and angles are listed in Table 3. Structural features of the $[Pt(bpy)_2]^+$ monocation of $[Pt(bpy)_2]NO_3 \cdot 2H_2O$ are strikingly similar to those of the $[Pt(bpy)_2]^{2+}$ dication of $[Pt(bpy)_2](NO_3)_2 \cdot H_2O$.[45] The reduction of $[Pt^{II}(bpy)_2]^{2+}$ to $[Pt^{I}(bpy)_2]^+$ is accompanied by little change in coordination geometry, which is consistent with the addition of charge to a metal out-of-plane orbital. (The addition of an electron to the in-plane ligand-field destabilized orbital ($d_{x^2-y^2}$) would likely result in major change.) The planes of pyridine rings associated with a common ligand are twisted by 7.5° to relieve overcrowding between hydrogen atoms at the C3 carbon atoms of bonded pyridine rings. In an ideally planar coordination geometry, hydrogen atoms bonded to the C6 ring carbon atoms would be in too close proximity. As a result, there is a twist in the coordination geometry to give a "crushed tetrahedron" with a dihedral angle between ligand planes of 34.4°.

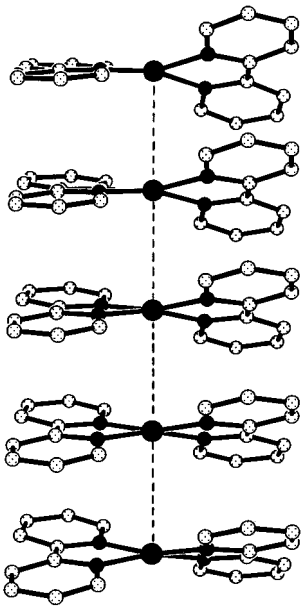

Figure 4. Crystal packing diagram of $[Pt^{I}(bpy)_2](NO_3) \cdot 2H_2O$ perpendicular to the stacking axis.

Table 3. Bond Lengths (Å) and Angles (deg) for $[Pt(bpy)_2](NO_3) \cdot 2H_2O$[a]

Bond Lengths			
Pt−N1	2.029(7)	C3−C4	1.347(18)
N1−C2	1.365(10)	C4−C5	1.377(19)
N1−C6	1.350(11)	C5−C6	1.380(17)
C2−C2A	1.444(18)	N2−01	1.027(178)
C2−C3	1.407(14)		
Angles			
N1−Pt−N1A	102.4(4)	N1−C5−C5	121.7(9)
N1−Pt−N1B	79.2(4)	C2−N1−C6	117.9(8)
N1−Pt−N1C	166.7(6)	C2−C3−C4	120.2(10)
Pt−N1−C2	115.7(5)	C3−C2−C2A	123.9(6)
Pt−N1−C6	125.7(6)	C3−C4−C5	118.6(11)
N1−C1−C3	121.0(9)	C4−C5−C6	120.5(10)
N1−C1−C2A	114.7(4)		

[a] Numbers in parentheses are estimated standard deviations in terms of least significant digits.

The most significant structural difference between $[Pt^{I}(bpy)_2]NO_3 \cdot 2H_2O$ and $[Pt^{II}(bpy)_2](NO_3)_2 \cdot H_2O$ crystals is revealed by their respective packing diagrams, which are shown in Figures 4 and 5. The crystal structure of $[Pt^{I}(bpy)_2](NO_3) \cdot 2H_2O$ consists of segregated chains of $[Pt(bpy)_2]^+$ cations and NO_3^- anions (Experimental Section). The anions are linked by hydrogen bonded water molecules. Complex cations stack atop one another, in a linear fashion, with adjacent molecules related by translational crystallographic symmetry about the *a* axis (molecular axis). The Pt−Pt separation is 3.563(1) Å as are the separations between all translationally related atoms. This distance is typical for the separation between stacked bipyridyl ligands of adjacent complex molecules. The Pt−Pt separation is long for complexes of Pt^{I}, where the formation of a relatively short Pt−Pt bond usually occurs to give a discrete dimer.[29−33] In the present case, bipyridyl−bipyridyl contacts restrict the extent to which adjacent metal atoms can approach one another, and define the separation between complex units within columnar stacks. The effect of planar diimine ligand interactions

(43) Cahen, D.; Lester, J. E. *Chem. Phys. Lett.* **1973**, *18*, 108.
(44) Tourillon, G.; Dartyge, E.; Palmans, R.; Frank, A. J. *Phys. B* **1989**, *158*, 208.
(45) Hazell, A.; Simonsen, O.; Wernberg, O. *Acta Crystallogr.* **1986**, *C42*, 1707.

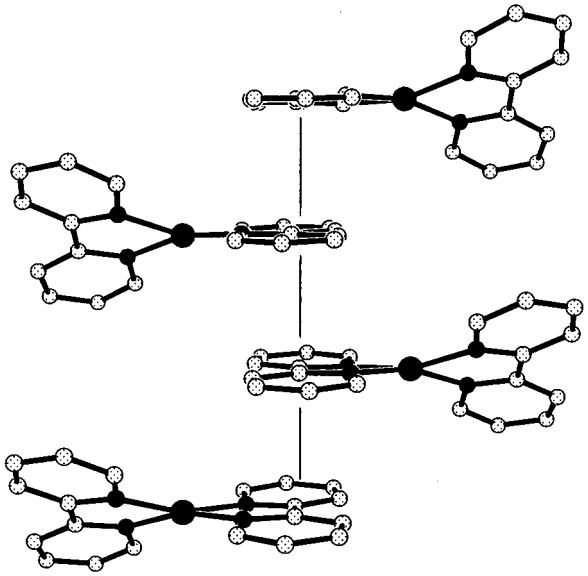

Figure 5. Crystal packing diagram of $[Pt^{II}(bpy)_2](NO_3)_2 \cdot H_2O$ perpendicular to the stacking axis (data from ref 45).

on metal−metal distance is also evident in discrete dimers.[46] The crystal structure of $[Pt^{II}(bpy)_2](NO_3)_2 \cdot H_2O$ consists of slipped stacks of complex cations paired by interactions between individual bipyridyl ligands as shown in Figure 5. The separation between planes of paired ligands is 3.55 Å, close to the separation between units in the $[Pt(bpy)_2]^{+}$ stack. None of the structure determinations on compounds containing the $[M(bpy)_2]^{2+}$ (M = Pd, Pt) cations have shown stacked structures with adjacent metals atop one another.[45] However, this feature appears commonly for complexes containing partially oxidized, planar platinum cations and anions, and complexes of Pt^{III}.[47]

The arrangement of $[Pt^{I}(bpy)_2](NO_3) \cdot 2H_2O$ appears to be the first example of a one-dimensionally stacked complex of Pt^{I}. The stacking interaction may be important in stabilizing Pt^{I} with a drop in energy of the metal p_z orbital that take place with stack formation;[48] π acceptors, such as bipyridine, are expected to lower the energy of the orbital. Participation of the Pt $6p_z$ orbital has been invoked to account for the positive reduction potential of chloro(terpyridine)platinum(II)[49] and Pt−Pt interactions in other compounds.[50] The addition of an electron to this out-of-plane orbital would also account for the structural similarity of $[Pt^{I}(bpy)_2]^{+}$ and $[Pt^{II}(bpy)_2]^{2+}$ discussed above and explain the basis for the relatively high conductivity of $[Pt^{I}(bpy)_2]NO_3 \cdot 2H_2O$ discussed below.

Electronic absorption measurements of $[Pt^{I}(bpy)_2]NO_3 \cdot 2H_2O$ crystals in solution were not possible. In deaerated polar solvents, such as water, ethanol, and acetonitrile, dissolution of the crystals led to a loss of their black-green color, indicating that the color arises from solid-state effects. In the solid state, electronic interactions between monomeric $[Pt(bpy)_2]$ units in molecular chains of Pt^{I} crystals are observable as a broad absorption band, spanning a wavelength range of at least 500−2500 nm, with a peak maximum centered at 1050 nm and an accompanying shoulder at 1500 nm in the diffuse-reflectance spectrum of $[Pt(bpy)_2]NO_3 \cdot 2H_2O$ (Figure 6). The absence of

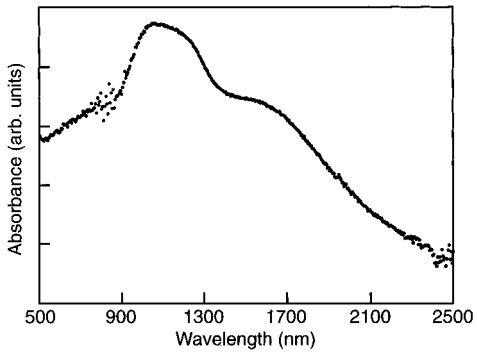

Figure 6. Diffuse reflectance spectrum of randomly oriented crystals of $[Pt^{I}(bpy)_2](NO_3) \cdot 2H_2O$.

this band in the spectrum of the dissolved crystals implies that it is associated with solid-state effects. In contrast, the diffuse-reflectance spectrum of $[Pt^{II}(bpy)_2](NO_3)_2 \cdot H_2O$ crystals exhibits the same absorption onset in the visible region (λ < 500 nm) as monomeric $[Pt(bpy)_2]^{2+}$ in aqueous solution,[51] suggesting no substantial solid-state effects. The different spectral characteristics of Pt^{I} and Pt^{II} crystals can be understood from their crystallographic packing diagrams (Figures 4 and 5). It can be seen that the degree of solid-state interaction in Pt^{I} crystals is likely to be much more extensive than that in Pt^{II} crystals. Specifically, Pt^{I} crystals consist of an infinite collection of face-to-face fully overlapping bipyridyl ligands in a single linear-chain structure with a Pt−Pt distance of 3.563 Å. In the Pt^{II} crystals, on the other hand, because of the slipped-stack nature of the linear-chain structure, only one of the bipyridyl ligands on each Pt center overlaps with its nearest neighbors. The Pt−Pt distance (>6.7 Å) between nearest or next-to-the-nearest neighboring $[Pt(bpy)_2]^{2+}$ units (Figure 5) is too large for metal−metal interaction. The overlapping bipyridyl ligands in the Pt^{II} structure also do not appear to lead to significant interaction as judged by the absence of new absorption features in the electronic spectrum of the solid. Moreover, the emission spectrum of Pt^{II} crystals does not support major ligand−ligand interaction. The emission spectrum of monomeric $[Pt(bpy)_2]^{2+}$ in a methanol/ethanol glass at 77 K[52] is very similar to that of the microcrystalline perchlorate salt of $[Pt(bpy)_2]^{2+}$ at 30 K,[51] indicating minimal perturbation of the monomeric electronic structure by crystalline packing.

The near-IR spectral features in the absorption spectrum of Pt^{I} crystals (Figure 6) can arise from either Pt−Pt or interligand interaction along the molecular chain. Because there is no spectral evidence for solid-state effects in Pt^{II} crystals, it is tempting to dismiss the possibility that interligand interaction accounts for the near-IR spectrum of Pt^{I} crystals in view of the fact that the distance between adjacent and overlapping bipyridyl ligands is comparable in both Pt^{I} and Pt^{II} crystals. However, this possibility cannot be excluded because, as the packing diagrams (Figures 4 and 5) show, the orientation of neighboring bipyridyl ligands is not the same in both crystals. In the Pt^{I} crystal, neighboring bipyridyl ligands overlap face-to-face with the N atoms of the ligands aligned along a common axis, whereas in the Pt^{II} crystal the overlapping bipyridyl ligands are rotated, relative to each other, by 180° such that the N atoms of nearest neighboring bipyridines are not aligned along a common axis. Alternatively, Pt−Pt interaction at a distance of 3.563 Å may be important. Linear-chain materials, comprising square-planar Pt^{II} complexes, with intermetallic distances of about 3.6 Å or less can display a solid-state spectrum that differs

(46) Chern, S.-S.; Liaw, M.-C.; Peng, S.-M. *J. Chem. Soc., Chem. Commun.* **1993**, 359.
(47) Hoffman, B. M.; Martinsen, J.; Pace, L. J.; Ibers, J. A. In *Extended Linear Chain Compounds*; Miller, J. S., Ed.; Plenum Press: New York, 1983; Vol. 3, p 459.
(48) Hoffmann, R. *Angew. Chem., Int. Ed. Engl.* **1987**, *26*, 846.
(49) Hill, M. G.; Bailey, J. A.; Miskowski, V. M.; Gray, H. B. *Inorg. Chem.* **1996**, *35*, 4585.
(50) Aullón, G.; Alemany, P.; Alvarez, S. *Inorg. Chem.* **1996**, *35*, 5061.
(51) Miskowski, V. M.; Houlding, V. H. *Inorg. Chem.* **1989**, *28*, 1529.
(52) Craig, C.; Watts, R. J. University of California at Santa Barbara. Personal communication.

from that of the monomer in solution.[1,3] This solid-state band has been ascribed to the d_{z^2}–p_z transition, with a possible contribution from metal-to-ligand charge transfer. The lowering of the energy of the p_z orbital by bonding formation, as discussed above, is consistent with the d_{z^2}–p_z transition being responsible for the low energy (near-IR) absorption features observed for Pt^I crystals. Likewise, in several interacting (face-to-face) square planar platinum(II) dimers, the d_{z^2}–p_z transition is lowest in energy.[49,53]

The perpendicular growth pattern of $[Pt^I(bpy)_2](NO_3)\cdot 2H_2O$ crystals indicates that they are conductive and that charge transport occurs along the molecular axis. The electrical conductivity of Pt^I crystals, grown either on a Pt electrode or on an iron wire, was the same, about 10 Ω^{-1} cm^{-1},[54] consistent with their having the same crystallographic structure. This value is comparable to that of other linear-chain materials, such as the partially oxidized (nonstoichiometric) tetracyanoplatinate salt $K_{1.75}[Pt(CN)_4]\cdot 1.5H_2O$.[19] The conductivity of Pt^I crystals is 10^{11} times higher than that of $[Pt^{II}(bpy)_2](NO_3)_2\cdot H_2O$ (10^{-10} Ω^{-1} cm^{-1}), indicating the importance of crystal structure and possible charge delocalization along the molecular axis. The low conductivity of Pt^{II} crystals is consistent with no significant metal−metal or ligand−ligand interaction, although, in the latter case, neighboring bipyridyl ligands do overlap. Charge transport through the linear-chain Pt^I structure probably involves overlapping partially filled p_z orbitals of the metal centers or an extended π-bonded system, resulting from overlapping bipyridyl ligands. The electrical conductivity of air-oxidized Pt^I crystals (1.3×10^{-7} Ω^{-1} cm^{-1}) is 10^8 times less than that of Pt^I crystals or 10^3 times greater than that of the original $[Pt^{II}(bpy)_2](NO_3)_2\cdot H_2O$. The reaction of O_2 with the Pt^I crystals disrupts the structural stacking arrangement as is evident by the decrease of crystallinity that occurs when crystals are exposed to air. Thus, the residual conductivity of air-oxidized Pt^I crystals may result from partial retention of the Pt−Pt core upon oxidation, a different conduction mechanism that may involve a new anion formed by the air-oxidation reaction, or a partially oxidized material that contains nonstoichiometric charge for the Pt ions.

(53) Roundhill, D. M.; Gray, H. B.; Che, C.-M. *Acc. Chem. Res.* **1989**, *22*, 55.

(54) The measured values may underestimate the conductivity of $[Pt(bpy)_2]NO_3\cdot 2H_2O$ by as much as one order of magnitude because the hollow nature of the crystals was not taken into consideration in the calculation.

Final Remarks

We have discovered a linear-chain d^9 Pt^I with a microtubular morphology. Crystallographic measurements along with other studies have provided a basis for understanding the relationship between the chemical structure of the repeating units of the linear-chain complex $[Pt^I(bpy)_2]NO_3\cdot 2H_2O$ and its physical properties—notably, its optical and electrical characteristics. Such an understanding may enable the electronic and mechanical properties of this compound or related materials to be tailored at the molecular level. The hollow nature of the crystalline needles derived from such materials and the ease with which they can be formed from discrete molecular species suggest, as discussed in this article, the possibility of combining and exploiting anisotropic properties of linear-chain transition-metal complexes with a tubular macroscopic structure.

Acknowledgment. We are grateful to Mr. V. Carperos at the University of Colorado for crystallographic measurements and to Dr. M. D. Ward at the University of Minnesota, Dr. R. B. Goldfarb at the National Institute of Standards and Technology, Dr. J. S. Miller at the University of Utah, Dr. G. T. Yee at the University of Colorado, and Drs. X. Gao and J. A. Turner at NREL for their valuable comments. This work was supported by the Hydrogen Program of the Office of Utility Technology (D.B.M.) and the Office of Basic Energy Sciences, Division of Chemical Sciences (A.J.F.), U. S. Department of Energy, under Contract DE-AC02-36CH10093.

Supporting Information Available: Tables of atomic coordinates and equivalent isotropic displacement parameters, anisotropic displacement parameters, and hydrogen atom coordinates and isotropic parameters for $[Pt(bpy)_2]NO_3\cdot 2H_2O$ (2 pages). See any current masthead page for ordering and Internet access instructions.

JA962491M